Neural, Parallel, and Scientific Computations 25 (2017) 497-507

ON THE NUMERICAL SOLUTIONS OF 2D BOUSSINESQ EQUATIONS WITH FRACTIONAL DISSIPATION

RAMJEE SHARMA

Department of Mathematics, University of North Georgia, Oakwood, Georgia 30566, USA

ABSTRACT. This paper presents the numerical computations of 2D Boussinesq equations with fractional dissipation. A parallel pseudospectral method is developed and implemented for the computation. Given smooth initial data, whether the solutions of the system with all the possible values of the parameters develop finite time singularity or not is yet to be known. This issue is addressed by presenting the evolution of geometry of the level curves, energy spectra and associated norms of two major quantities involved in the system. The solutions were computed for different values of parameters. Some of the numerical solutions presented here strongly indicate potential singularity in finite time suggesting a need for further investigations.

AMS (MOS) Subject Classification. 39A10.

1. INTRODUCTION

The 2D Boussinesq equations with fractional dissipation are given by

$$\begin{cases} \partial_t u + u \cdot \nabla u = -\nabla p - \nu(\Lambda)^\alpha u + \theta e_2, \\ \partial_t \theta + u \cdot \nabla \theta + \kappa(\Lambda)^\beta \theta = 0, \\ \nabla \cdot u = 0, \end{cases} \tag{1.1}$$

where $u = (u_1, u_2)$ is the velocity field, p is the pressure and θ is a scalar quantity carried by the fluid. The real numbers $\nu \geq 0, \quad \kappa \geq 0, \quad 0 < \alpha \leq 2, \quad 0 < \beta \leq 2$ are parameters, and the vector $e_2 = (0, 1)$. The Zygmund operator $\Lambda = (-\Delta)^{\frac{1}{2}}$ is defined through the Fourier transform,

$$\widehat{\Lambda^\alpha f}(k) = |\xi|^\alpha \widehat{f}(k).$$

Using $\omega = \nabla \times u$, equations (1.1) can be written as

$$\begin{cases} \partial_t \omega + u \cdot \nabla \omega = -\nu(\Lambda)^\alpha \omega + \partial_{x_1} \theta, \\ \partial_t \theta + u \cdot \nabla \theta + \kappa(\Lambda)^\beta \theta = 0, \\ \nabla \cdot u = 0, \end{cases} \tag{1.2}$$

where u can be recovered by the relation $u = \nabla^\perp \Delta^{-1} \omega$.

Received April 18, 2017

The main issue regarding the equations (1.1) is: given $u(x,0) = u_0(x)$, and $\theta(x,0) = \theta_0(x)$, which are both smooth and approach 0 at infinity, does the Boussinesq system (1.1) have a global classical solution in time. When $\alpha = \beta = 2$, (1.1) reduces to the standard Boussinesq equations with Laplacian dissipation. The standard Boussinesq equations model geophysical flows such as atmospheric fronts and oceanic circulation, and also play an important role in the study of Raleigh-Bernard convection. The global regularity in this case can be established using the same methods as for the 2D Navier-Stokes equations [12]. When there is no dissipation, namely $\nu = \kappa = 0$ in (1.1), the global regularity problem is open. Several important findings have been made in the recent years in this case. Authors in ([5] and [6]) established global well-posedness results of 2D Boussinesq equations with fractional diffusion. In particular, the solutions of (1.1) has global classical solutions when $\alpha = 2$ and $\kappa = 0$ or when $\beta = 2$ and $\nu = 0$ ([3] and [10]). Additionally, the authors in ([19] and [20]) independently extended these results to higher dimensions. Recently, Stefanov and Wu in [13] established the global existence and smoothness of classical solutions of (1.1) for $\alpha > \frac{\sqrt{1777}-23}{24} = 0.798103..$, $\beta > 0$ and $\alpha + \beta = 1$. The main goal of this paper is to study the open case $\alpha + \beta = 1$ and $\alpha < 0.798$ through rigorous numerical computations. The spatial domain used in the computations here is the periodic box $[0, 2\pi]^2$.

Because of the periodic boundary conditions used in the computations, the pseudospectral scheme appears to be the most suitable method (see, e.g. [4]). More precisely, we approximate the solutions θ and ω in (1.2) by $\tilde{\theta}$ and $\tilde{\omega}$ in the following forms.

$$\tilde{\theta}(x,t) = \sum_{k_1,k_2=-N/2}^{N/2-1} \hat{\theta}(k_1,k_2) e^{ik\cdot x},$$

$$\tilde{\omega}(x,t) = \sum_{k_1,k_2=-N/2}^{N/2-1} \hat{\omega}(k_1,k_2) e^{ik\cdot x},$$

where $\hat{\theta}$ and $\hat{\omega}$ are the Fourier transforms of θ and ω respectively, namely

$$\hat{\theta}(k_1,k_2) = \frac{1}{(2\pi)^2} \int_{T^2} \theta(x_1,x_2) e^{-i(k_1x_1+k_2x_2)} dx_1 dx_2$$

$$\hat{\omega}(k_1,k_2) = \frac{1}{(2\pi)^2} \int_{T^2} \omega(x_1,x_2) e^{-i(k_1x_1+k_2x_2)} dx_1 dx_2$$

and N is a fixed integer given by $N = 2^m$ for some integer m. A parallel algorithm for the pseudospectral method was developed and implemented to compute the solutions. These computations reveal detailed finite time behavior, large-time asymptotic and key parameter dependence of the solutions and provide valuable information for further investigations on the global regularity issue concerning the Boussinesq equations.

2. **Numerical Solution Scheme**

In this section, the numerical method is developed for the equations (1.2). Fourier transforms of the first two equations in (1.2) yield

$$\widehat{\partial_t\omega} + \widehat{u_1\omega_{x_1}} + \widehat{u_2\omega_{x_2}} = -\nu\widehat{(\Lambda)^\alpha\omega} + \widehat{\partial_{x_1}\theta},$$
$$\widehat{\partial_t\theta} + \widehat{u_1\theta_{x_1}} + \widehat{u_2\theta_{x_2}} = -\kappa\widehat{(\Lambda)^\beta\theta}.$$

The condition $\nabla \cdot u = 0$ further reduces the equations to

$$\widehat{\partial_t\omega} + \widehat{(u_1\omega)_{x_1}} + \widehat{(u_2\omega)_{x_2}} = -\nu\widehat{(\Lambda)^\alpha\omega} + \widehat{\partial_{x_1}\theta},$$
$$\widehat{\partial_t\theta} + \widehat{(u_1\theta)_{x_1}} + \widehat{(u_2\theta)_{x_2}} = -\kappa\widehat{(\Lambda)^\beta\theta}.$$

After taking the Fourier transform of the space derivatives, these equations are converted into the following equations.

$$\widehat{\partial_t\omega} + ik_1\widehat{(u_1\omega)} + ik_2\widehat{(u_2\omega)} = -\nu|k|^\alpha\widehat{\omega} + ik_1\widehat{\theta}$$
$$\widehat{\partial_t\theta} + ik_1\widehat{(u_1\theta)} + ik_2\widehat{(u_2\theta)} = -\kappa|k|^\beta\widehat{\theta}$$

Finally, the time derivative of ω and θ can be expressed as

$$\widehat{\partial_t\omega} = -ik_1\widehat{(u_1\omega)} - ik_2\widehat{(u_2\omega)} - \nu|k|^\alpha\widehat{\omega} + ik_1\widehat{\theta},$$
$$\widehat{\partial_t\theta} = -ik_1\widehat{(u_1\theta)} - ik_2\widehat{(u_2\theta)} - \kappa|k|^\beta\widehat{\theta}.$$

As seen above, the space derivatives are calculated in the Fourier space. The nonlinear terms $u_1\omega$, $u_2\omega$, $u_1\theta$ and $u_2\theta$ are computed in the physical space. The time integration is carried out by fourth-order Runge-Kutta method.

The same smooth initial conditions were used for both θ and ω. These are the same initial condition used by the authors in [1] as given below.

$$\omega(x_1, x_2, 0) = \theta(x_1, x_2, 0) = \sin(x_1)\sin(x_2) + \cos(x_2) \tag{2.1}$$

These initial data represent the simplest type of smooth initial data with nonlinear behavior.

3. **Parallelization Scheme**

Standard mpi routines were used to communicate among the processes. Matrix parallelization was carried out by slab decomposition. For example, if there are N rows and p workers (processes 1 through p) along with one master (process 0), then the process 0 will distribute $\frac{N}{p}$ rows to each process. The remaining rows (mod (N, p)) are handled by the process 0 itself. Each process then completes its part of the job

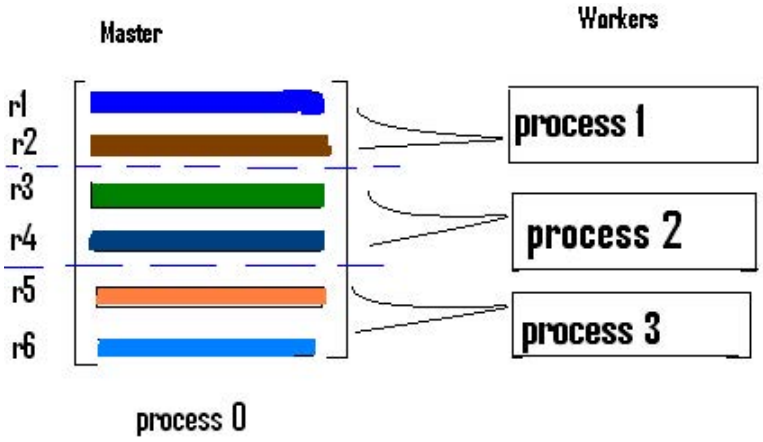

FIGURE 1. Parallelization through slab decomposition

and sends it back to the process 0. Figure (1) depicts the process for a matrix with six rows and four processes (process 0,1,2,3).

All the computations were done on Intel Pentium Xeon EM64T quad Core E5405 @ 2.0 GHz processors in Cowboy Super Computing Center, Oklahoma State University, Stillwater, OK. A total of 128 machines were used with uniform mesh sizes up to 4096×4096. The Fourier transform process was parallelized by utilizing the parallelized mpi fftw routines.

4. **Exponential Filter**

In order to reduce the aliasing errors in the computation, the Fourier multipliers ik_j for the differential operator $\frac{\partial}{\partial x_j}$ were used to obtain $ik_j\phi(|k_j|)$, where

$$\phi(k) = e^{-\eta}(\frac{k}{N})^{m_f}$$

for $|k| \leq N$. Here N is the numerical cutoff for the Fourier modes, and m_f is the order of the filter. The value of α was so chosen that $\phi(N) = e^{-\eta}$=machine epsilon. For a smooth function $f(x)$,

$$||f(x) - D_N f(x)|| = O(N^{-m_f}),$$

where $D_N f = F^{-1}(ik\phi(|k|)F(f))$ is the numerical approximation of $f'(x)$. F denotes the Fourier transform operator. For the purpose of these computations, $e^{-\eta}$=machine accuracy=2.2204 e-16 was used. Therefore, $\eta = -\ln(2.2204e-16) = 36.0437$. Unlike in the conventional 2/3 rd dealiasing method where the higher frequency modes are replaced by zeros, this method suppresses the higher frequency modes but keeps some of the information. Figure 2 portrays the graph of a sample exponential filter.

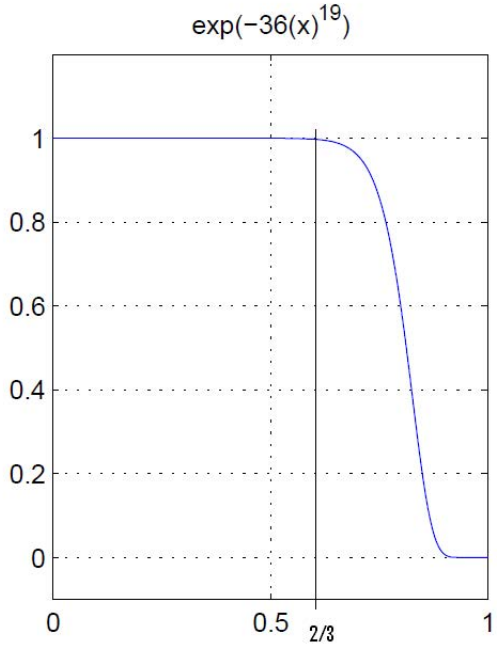

FIGURE 2. Exponential filter

5. **Error Analysis of the Method**

Unlike in the 3-point finite difference method or five points finite difference methods, the pseudospectral method uses N-points formulas. As for example, for N=10, one would need a tenth order finite difference or finite element methods to achieve an error of $O(h^{10})$. As N increases, the pseudospectral method benefits in two different ways. First the interval h (the interval between the grid points) becomes smaller. This would cause the error to rapidly decrease even if the order of the method were fixed. Unlike finite difference and finite element methods, however, the order is not fixed. When N increases from 10 to 20, the error becomes $O(h^{20})$ in terms of the new smaller h. Since h is $O(1/N)$, in pseudospectral method, the error is of $O((1/N)^N)$. However, the errors from truncation and from the time integration are still in place.

Before the program was implemented to the actual system (1.2), it was implemented to the following linearized problem along with the initial condition $\omega(x_1, x_2, 0)$ given in (2.1). The linearization was done by putting $u_1 = 1, u_2 = 1, \nu = 0, \kappa = 0$, and $\theta = 0$. In this case the system converts to the transport equation

$$\partial_t \omega + \partial_{x_1} \omega + \partial_{x_2} \omega = 0. \tag{5.1}$$

The exact solution of (5.1) is given by

$$\omega(x_1, x_2, t) = \omega_0(x_1 - t, x_2 - t).$$

L^2 norms and L^∞ norms of the computed solution were compared with those of the exact solutions. Figure 3 represents the spectra of the computed solutions and

those of the exact solutions side by side from time $t = 1$ to $t = 10$. For the same time interval, the L^2 and L^∞ errors of ω are presented in Table 1.

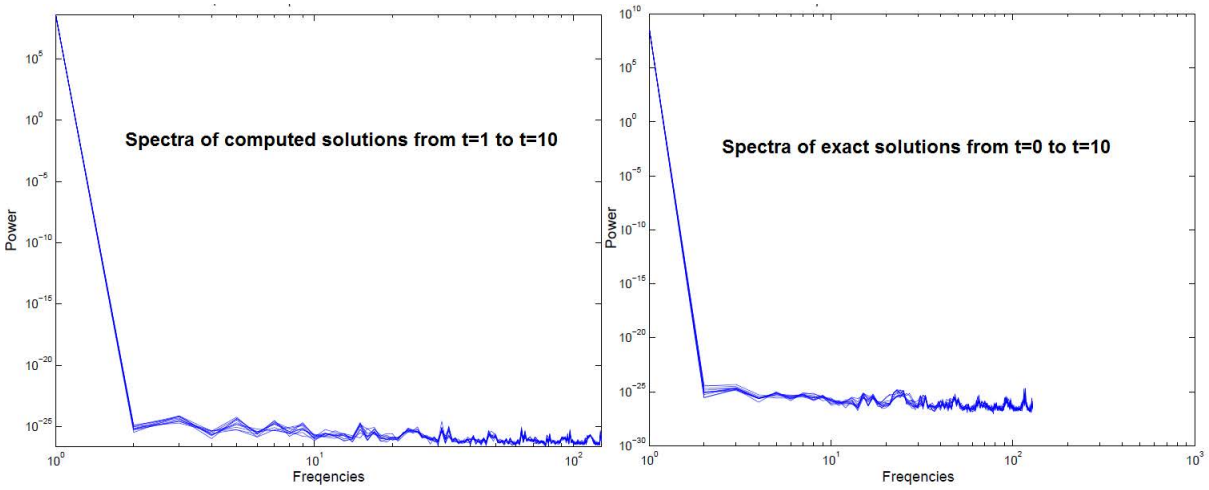

FIGURE 3. Spectra of exact and computed solutions from $t = 1$ to $t = 10$

time (t)	L^2 error of ω	L^∞ error of ω
1	1.1593e-006	2.1461e-006
2	2.3186e-006	4.0945e-006
3	3.4779e-006	6.2720e-006
4	4.6373e-006	8.5361e-006
5	5.7966e-006	1.0739e-005
6	6.9559e-006	1.2309e-005
7	8.1153e-006	1.4724e-005
8	9.2746e-006	1.7105e-005
9	1.0434e-005	8.5361e-006
10	1.1593e-005	1.9344e-005

TABLE 1. L^2 and L^∞ errors of ω

6. **Numerical Results**

This section presents the results from the numerical computations in the form of level curves, energy spectra and norms of θ and ω. The study was carried out by varying the values of the parameters α, β, ν and κ at different values. These computational results show that the geometry of level curves as well as the growth of norms depend on the values of the key parameters used in the equations. During the evolution of the numerical solutions, the quantities $||\omega||_2, ||\omega||_\infty, ||\theta||_2$ and $||\theta||_\infty$ were recorded and closely monitored. The time step Δt used was small enough to meet the CFL condition.

The computation was done in two parts. In the first part, the value of α was set to 0.6 and that of $\beta = 1 - \alpha$. The values of ν and κ were set to 0.2 throughout the computations. The regions where the level curves come close to each other were monitored in order to predict potential finite time singularity of the solutions. Level curves and norms of ω and θ at different times are presented here. Figure 4 shows the level curves of θ and ω at $t = 0$. Figure 5 represents the level curves of ω and θ from time $t = 1$ to $t = 10$. Likewise, Table 2 shows the evolution of L^2 and L^∞ norms of θ and ω from $t = 0$ to $t = 10$.

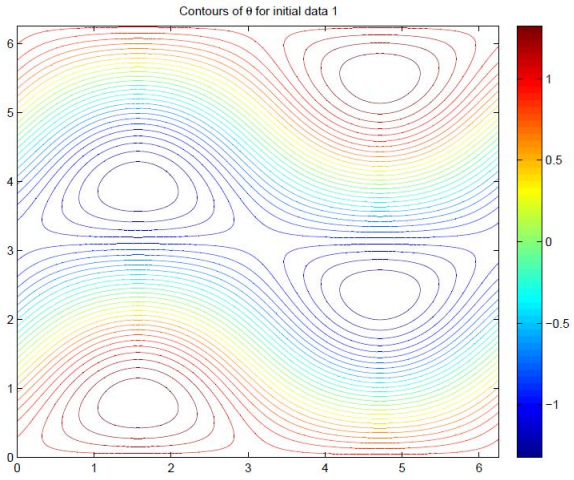

FIGURE 4. Initial level curves of both θ and ω

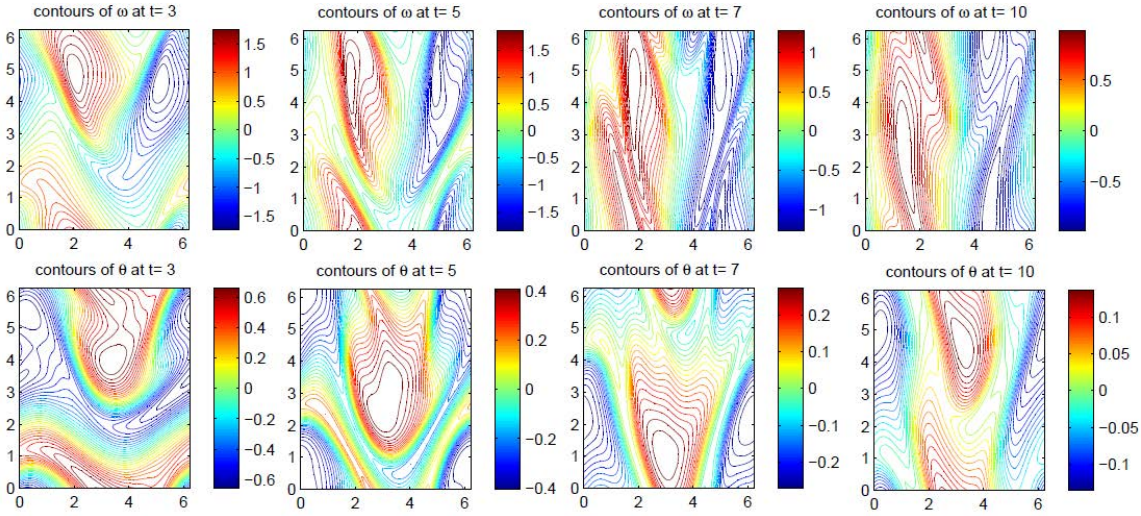

FIGURE 5. Level curves of ω and θ for $\alpha = 0.6$, $\beta = 1 - \alpha$ and $\nu = \kappa = 0.2$

In the second part of the computations, value of the parameter α was lowered to 0.4 with $\beta = 1 - \alpha$. The values of ν and κ were maintained at 0.2. The same initial data were used for this computation. The evolution of level curves and associated norms resulted from this round of computations are presented in the following graphs and tables. Figure 6 represents the level curves of ω and θ from time $t = 1$

time (t)	L^2 norm of ω	L^∞ norm of ω	L^2 norm of θ	L^∞ norm of θ
0	0.8660	1.4142	0.8660	1.4142
1	0.7835	1.3492	0.6942	1.1233
2	0.8050	1.5780	0.5533	0.8926
3	0.8660	1.8576	0.4320	0.7027
4	0.9453	2.0307	0.3285	0.5501
5	0.9658	1.9833	0.2487	0.4342
6	0.8979	1.7203	0.1928	0.3577
7	0.8180	1.3607	0.1515	0.2906
8	0.7616	1.2131	0.1185	0.2321
9	0.7061	1.1756	0.0930	0.1839
10	0.6422	1.0488	0.0737	0.1452

TABLE 2. Norms of ω and θ for $\alpha = 0.4$, $\beta = 1 - \alpha$ and $\nu = \kappa = 0.2$

to $t = 10$. In order to understand the behavior of the solutions in the Fourier space, power spectra of ω and θ are also presented here. Figure 7 represents spectra of ω and θ averaged over angles from time $t = 1$ to $t = 10$. For these values of the parameters, the level curves seem to have come much closer at times, but the regions vary as the time goes on. The L^2 and L^∞ norms of θ and ω are presented in Table 3.

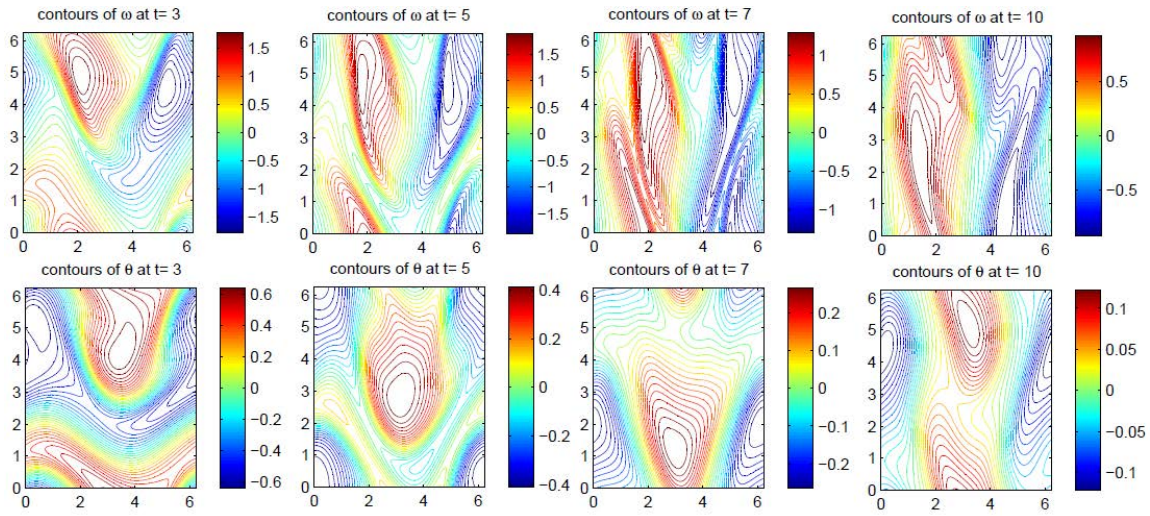

FIGURE 6. Level curves of ω and θ for $\alpha = 0.4$, $\beta = 1 - \alpha$ and $\nu = \kappa = 0.2$

7. **Conclusion**

The approximate solutions of equations (1.2) corresponding to the parameters $\alpha = 0.6$, $\beta = 1 - \alpha$ and $\nu = \kappa = 0.2$ do not seem to develop finite time singularities

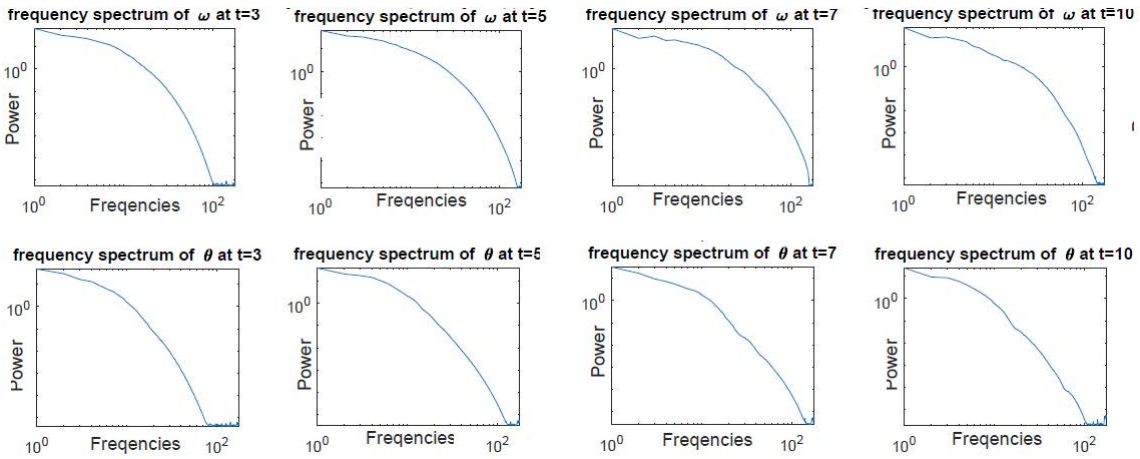

FIGURE 7. Energy spectra of ω and θ for $\alpha = 0.4$, $\beta = 1 - \alpha$ and $\nu = \kappa = 0.2$

time (t)	L^2 norm of ω	L^∞ norm of ω	L^2 norm of θ	L^∞ norm of θ
0	0.8660	1.4142	0.8660	1.4142
1	0.7908	1.3692	0.6858	1.1048
2	0.8137	1.6154	0.5391	0.8695
3	0.8715	1.8990	0.4113	0.6834
4	0.9423	2.0692	0.3021	0.5417
5	0.9585	2.0132	0.2237	0.4390
6	0.8898	1.7429	0.1749	0.3559
7	0.7971	1.3871	0.1380	0.2827
8	0.7273	1.1546	0.1065	0.2200
9	0.6675	1.0808	0.0826	0.1694
10	0.6044	1.1546	0.0654	0.1302

TABLE 3. Norms of ω and θ for $\alpha = 0.4$, $\beta = 1 - \alpha$ and $\nu = \kappa = 0.2$

for the type of initial condition used in the computations. Both the norms are under control in this case. On the other hand, level curves of ω and θ corresponding to $\alpha = 0.6$, $\beta = 1 - \alpha$ and $\nu = \kappa = 0.2$ come closer and closer at various regions of the computational domain. The L^∞ norm of ω seem to slightly increase around $t = 4$, but starts to decrease after that until $t = 10$. While the norms of θ are still under control, these strange behavior of the solutions of ω imply the need for further numerical computations, and theoretical and geometric analysis in order to better understand whether the solutions develop any type of singularities in finite time or not. The Fourier modes are well resolved in both rounds of computations.

ACKNOWLEDGMENTS

The author would like to sincerely thank Dr. Jiahong Wu, Professor of Mathematics, Oklahoma State University for his continuous guidance, and invaluable help and support. The author also would like to thank Dr. Dana Brunson, director of Cowboy High Performance Computing Center, Oklahoma State University for generously providing with the computing facility.

REFERENCES

[1] P. Constantin, M.-C. Lai, R. Sharma, Y.-H. Tseng, J. Wu, New numerical results for the surface quasi-geostrophic equations, *Journal of Scientific Computing,* **50** (2012), No.1, 1-28.

[2] X. Cui, C. Dou and Q. Jiu, Local well-posedness and blow up criterion for the inviscid Boussinesq system in Hölder spaces, *J. Partial Differential Equations,* **25** (2012), 220238.

[3] D. Chae, Global regularity for the 2D Boussinesq equations with partial viscosity terms, *Adv. Math,* **203** (2006), 497513.

[4] D. Gottlieb, S.A. Orszag, S.A, Numerical Analysis of Spectral Methods: Theory and Applications, *CBMSNSF, Regional Conference Series in Applied Mathematics* vol. 26. SIAM, Philadelphia (1977)

[5] T. Hmidi, S. Keraani, F. Rousset, Global well-posedness for a Boussinesq-Navier-Stokes system with critical dissipation, *J. Differential Equations,* **249** (2010), 2147-2174.

[6] T. Hmidi, S. Keraani, F. Rousset, Global well-posedness for Euler-Boussinesq system with critical dissipation, *Comm. Partial Differential Equations,* **36** (2010), 420-445.

[7] Q. Jiu, C. Miao, J. Wu and Z. Zhang, The 2D incompressible Boussinesq equations with general critical dissipation, *SIAM J. Math. Anal.* **46** (2014), 3426-3454.

[8] Q. Jiu, J. Wu, and W. Yang, Eventual regularity of the two-dimensional Boussinesq equations with supercritical dissipation, *J. Nonlinear Science,* in press.

[9] K. Ohkitani, Comparison between the Boussinesq and coupled Euler equations in two dimensions, *Tosio Katos method and principle for evolution equations in mathematical physics* (Sapporo, 2001). Surikaisekikenkyusho Kokyuroku No. 1234 (2001), 127-145.

[10] T. Hou and C. Li, Global well-posedness of the viscous Boussinesq equations, *Discrete and Cont. Dyn. Syst.* **12** (2005), 1-12.

[11] A. Sarria and J. Wu, Blowup in stagnation-point form solutions of the inviscid 2d Boussinesq equations, *arXiv:1408.6625 [math.AP]* 28 Aug 2014.

[12] A. Majda, A. L. Bertozi, Vorticity and Incompressible Flow, *Cambridge University Press, Cambridge, U.K.* , 2001.

[13] A. Stefanov, J. Wu, A Global regularity result for the 2D Boussinesq Equations with critical dissipation, *arXiv:1411.1362v3 [math.AP]* 2 Mar 2015

[14] J. Wu, The 2D Boussinesq equations with partial or fractional dissipation, *Lectures on the analysis of nonlinear partial differential equations, Morningside Lectures in Mathematics, Edited by FangHua Lin and Ping Zhang, International Press, Somerville, MA,* 2014, in press.

[15] J. Wu and X. Xu, Well-posedness and inviscid limits of the Boussinesq equations with fractional Laplacian dissipation, *Nonlinearity* **27** (2014), 2215-2232.

[16] J. Wu, X. Xu, Z. Ye, Global regularity for several incompressible fluid models with partial dissipation, *J Math. Fluid Mechanics*, (2016), DOI 10.1007/s00021-016-0291-4.

[17] J. Wu, X. Xu and Z. Ye, Global smooth solutions to the n-dimensional damped models of incompressible fluid mechanics with small initial datum, *J. Nonlinear Science*, in press.

[18] W. Yang, Q. Jiu and J. Wu, Global well-posedness for a class of 2D Boussinesq systems with fractional dissipation, *J. Differential Equations* **257** (2014), 4188-4213.

[19] K. Yamazaki, On the global regularity of N-dimensional generalized Boussinesq system, *Appl. Math.,* **60** (2015), 103-133.

[20] Z. Ye, A note on global well-posedness of solutions to Boussinesq equations with fractional dissipation, *Acta Math. Sci. Ser. B Engl. Ed.,* **35B** (1) (2015), 112-120.